J-Researchers

Journal of Civil Engineering Researchers

Journal homepage: www.journals-researchers.com

Numerical Development of a Re-centering Damper with High Seismic Performance, Including Friction Wedges and SMA Rods

Jalal AkbarKamali,[a] Mahdi Mashhadiyan,[a,*] Esmaeil Mousapoor [a]

[a] *Department of Civil Engineering, Ramsar Branch, Islamic Azad University, Ramsar, Iran*

ABSTRACT

Re-centering dampers, developed using shape memory alloy (SMA)-based dampers and their superelasticity capability, absorb earthquake energy and provide a re-centering capability for the structure. In this study, the laboratory sample of Zhang's re-centering damper was first validated using ABAQUS software, followed by parametric analysis involving changes in the number and diameter of SMA rods, the friction coefficient of the wedges, and the placement configuration of two dampers, which were numerically investigated. The results indicated that increasing the diameter and number of rods, as well as the friction coefficient, enhances seismic resistance and stiffness but reduces ductility; excessive increase in friction only boosts the stiffness and ductility of the damper's compressive section while reducing seismic resistance. A friction coefficient of approximately 0.12 is recommended, whereas Zhang assumed 0.09. Additionally, the results showed: in parallel configuration, resistance and stiffness are higher but ductility is lower, whereas in series configuration, all three parameters decrease.

ARTICLE INFO

Received: November 18, 2025
Accepted: November 29, 2025

Keywords:
Numerical Development
Re-Centering Damper
SMA
Friction Wedge
Seismic Performance

DOI: 10.61186/JCER.7.4.68
DOR: 20.1001.1.22516530.1399.11.4.1.1

1. Introduction

Modern building codes can reduce base shear by employing a behavior factor (R), but conventional systems often result in permanent deformations and structural damage. To address this issue, dampers are utilized, as they absorb and dissipate input energy, reducing lateral displacements and applied forces, thereby enhancing safety, stability, and the service life of structures, particularly in seismic-prone areas where their necessity is greater [1]. A damper is a device used to absorb and dissipate energy from dynamic forces such as earthquakes or wind in structures, reducing vibrations and deformations, preventing damage to main members, and improving the seismic performance of the structure [2].

Re-centering dampers are an advanced type of damper used to reduce permanent deformations and restore the structure to its initial state after an earthquake. These dampers improve the seismic performance of the structure by absorbing energy and generating a restoring force, preventing damage to main members, and thus increasing building safety and stability [3]. Despite these advantages, challenges of re-centering dampers include complex design, nonlinear material behavior, high construction and

* Corresponding author. Tel.: +989111962921; e-mail: mahdi.mashhadiyan@gmail.com.

installation costs, sensitivity to temperature and environmental conditions, and a lack of laboratory data; nevertheless, they are highly effective in improving structural seismic performance [4]. Due to these limitations, their widespread application remains restricted. Researchers have addressed these issues by improving numerical modeling, conducting extensive experiments, and developing simpler, more economical designs with optimized materials and mechanisms to facilitate practical use in structures [5].

In recent years, shape memory alloys have garnered significant attention in civil engineering due to their superelasticity and ability to recover their original shape and dissipate energy, particularly in self-centering systems, with applications in bolts, steel elements, concrete rebars, braces, base isolators, and bridges [6]. The most prominent is nickel-titanium (Nitinol), used in civil engineering, aerospace, automotive, and medical fields due to its superelasticity and shape memory properties, though it has limitations such as fatigue, transformation temperature, and production costs [7]. However, SMA energy dissipation alone is insufficient for high-performance self-centering systems, leading to the design of hybrid dampers that combine SMA with friction wedges or metallic tools [8]. Studies show that SMA-based dampers can reduce permanent displacements and residual deformations in structures, absorb earthquake energy, and effectively control seismic vibrations in buildings and small bridges through self-re-centering without requiring repairs after severe earthquakes [9]. Recent research indicates that SMA superelastic rods and dampers exhibit stable hysteretic behavior and strong self-centering under cyclic loading [10]. Studies by Wang et al. with SMA rods and U-shaped dampers showed stable flag-shaped hysteretic loops, over 98% deformation recovery, and minor strain rate effects [11].

In this study, the numerical development of Zhang's re-centering dampers with high seismic performance, including friction wedges and SMA rods, will be investigated. First, nonlinear three-dimensional analysis using ABAQUS software [12] and cyclic seismic loading is performed, with model validation against experimental data. Subsequently, parametric studies examine the effects of the number and diameter of SMA rods, wedge friction coefficient, and the arrangement of two dampers (series or parallel) on the damper's resistance, stiffness, and ductility. The results demonstrate that these parameters play a crucial role in energy absorption capacity and damper performance, with numerical results and load-displacement diagrams illustrating the effects of parametric variables on the damper's seismic behavior.

2. Numerical Validation of the Curved Damper

In this study, to validate the finite element modeling and align numerical results with actual performance, experimental data from Zhang et al. [8] on a re-centering damper with friction wedges and SMA rods under quasi-static and cyclic compressive loading were used. Zhang et al. tested eight samples, and the selected sample for validation includes dimensional details of the wedges and SMA rods, presented schematically along with laboratory images in Figure 1. Cyclic compressive loading in the laboratory requires a specific pattern, so Figure 1 shows the compressive loading pattern for the studied re-centering damper with SMA rods. As per Figure 1, the compressive loading has 20 displacements, forming 10 back-and-forth compressive cycles in total, with the load applied via a hydraulic jack from the top to wedge No. 1, while wedge No. 2 has a support below it. According to the compressive loading pattern, the displacement ranges from 0.3 mm to 6.3 mm, only in compression. With damper displacement, the results are plotted as a compressive load-displacement hysteretic diagram, with load in kilonewtons and displacement in millimeters.

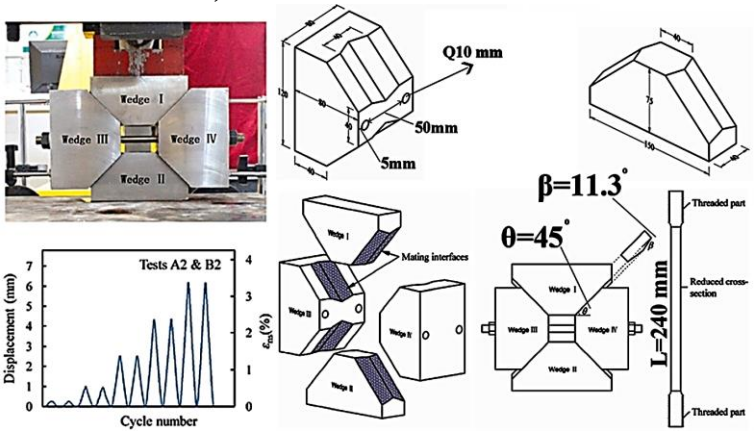

Figure 1- Dimensional characteristics of wedges and SMA rods used in compressive loading tests in Zhang et al. [8].

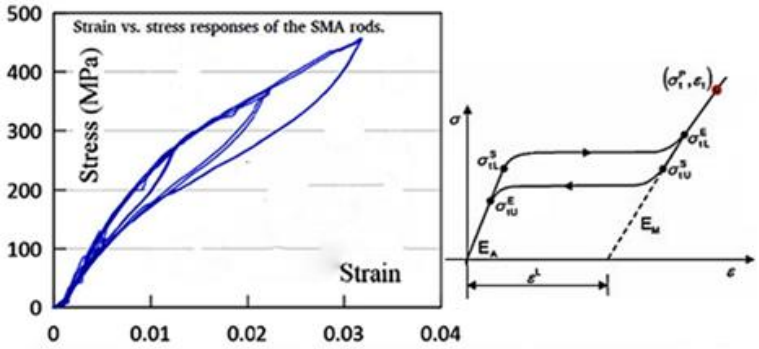

Martensite's Young's Modulus E_M	Martensite's Poisson's Ratio ϑ_M	Transformation Strain ε^L	Start of Transformation (Loading) σ_{StL}	End of Transformation (Loading) σ_{EtL}	Start of Transformation (Unloading) σ_{StU}	End of Transformation (Unloading) σ_{EtL}
3000000000 N/Pa	0.33	0.02	17000000 Pa	45000000 Pa	20000000 Pa	5000000 Pa

Figure 2- Sample display, diagram, and stress-strain values of the superelastic shape memory alloy rod from Zhang et al. [8].

As per Figure 1, the operation of the re-centering damper with SMA rods is as follows: This damper consists of 4 steel wedges (two vertical and two horizontal), two SMA rods, and 4 nuts. The vertical wedges (1 and 2) and horizontal wedges (3 and 4) interact on common contact surfaces (with frictional surfaces) and specific grooves. The damper operates generally as follows:

- In tension: When the damper is under tensile load, the backs of the vertical wedges (1 and 2) rest against the outer steel frame, and the tensile force is transferred through the frame. In this state, the SMA rods are not activated.
- In compression: When the damper is under compressive load, the vertical wedges (1 and 2) apply force to the horizontal wedges (3 and 4) at a 45-degree angle between the vertical and horizontal wedges, causing the SMA rods to stretch and engage, thus the damper performs and absorbs energy.

In summary, the wedges transfer axial forces to the SMA rods, and the damper primarily dissipates energy under compressive loads, while under tensile loads, the force is transferred through the outer steel frame.

In the continuation of this study, numerical analysis is performed to examine the performance of the shape memory alloy re-centering damper. The superelastic property and flag-shaped stress-strain diagram of the shape memory alloy material used in this study are shown in Figure 2. As per Figure 2, the stress-strain diagram of the superelastic SMA rod indicates that SMA materials exhibit no permanent deformation even with strains up to about 3% and return to their initial state after unloading. The elastic modulus of the superelastic SMA rod in the re-centering damper can be extracted from this diagram. Furthermore, Zhang explicitly stated that the steel used for all metallic components has a yield stress of 240 MPa, ultimate stress of 300 MPa, and elastic modulus of 200 GPa.

For validation, a numerical sample (matching the laboratory sample) was created in ABAQUS software to achieve similar results. The re-centering damper sample was modeled by creating four elements according to laboratory dimensions and assembling them. Steel and SMA rod properties were defined in the material properties module and assigned to the components. In ABAQUS (version 2019 and later), parameters such as Young's modulus, Poisson's ratio, start and end stresses of the material phases for the shape memory alloy in Zhang et al.'s [8] re-centering damper with SMA rods are defined, and material specifications are determined based on the stress-strain diagram (parameters from Figure 2) of the laboratory superelastic rod sample. As per Figure 3, for applying cyclic compressive load and defining boundary conditions, reference points at the top (for load application) and bottom (for support definition) are created with coupling constraints, and the two side surfaces of the sample are constrained in out-of-plane displacement and lateral movement. For interaction between the SMA rod and its nut, 4 fully tied constraints must be applied at 4 connections as per Figure 3. Additionally, in the numerical sample, for interaction between steel wedges and SMA rod and wedge sliding, surface contact must be defined with a friction coefficient of 0.088 between steel wedges and SMA rod.

To apply load and support conditions in ABAQUS's loading module, gravity loading is first defined for the sample, then the bottom surface is fixed as a clamped support in terms of displacement and rotation, while the upper coupling reference point is subjected to cyclic displacement-controlled compressive loading. With

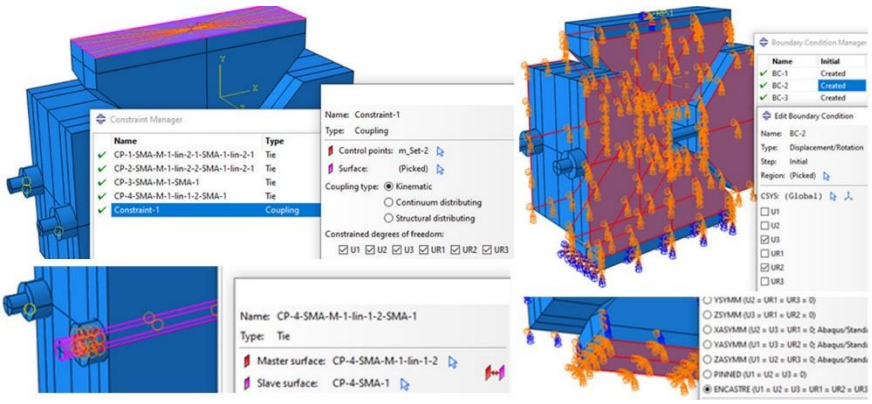

Figure 3- Sample display, diagram, and stress-strain values of the superelastic shape memory alloy rod from Zhang et al. [8].

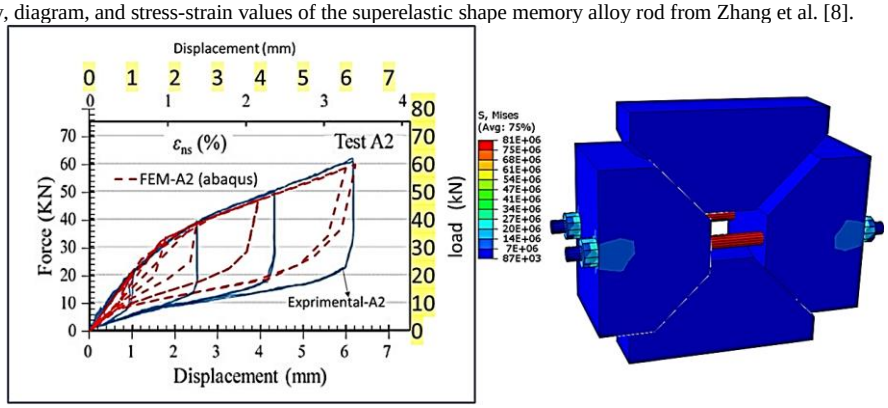

Figure 4- Stress results on the re-centering damper model – Alignment of numerical results with experimental results from Zhang et al. [8].

appropriate meshing (1 cm for wedges and 2 mm for rods), the numerical model is prepared, and the re-centering damper sample is analyzed using quasi-static analysis and applied loading. As per Figure 4, the von Mises stress results of the obtained sample after lateral loading and the load-displacement diagram indicate that the stress share in the SMA rod is higher than in other parts, and the hysteretic load-displacement diagram output confirms the re-centering behavior of the damper with a flag-shaped output. In the re-centering damper with SMA rods, compressive force is converted to tensile force in the rods, with maximum stress concentrated in the SMA rods, and the alignment of numerical and experimental results validates the model. Furthermore, as per Figure 5 in the compressive load-displacement hysteretic diagram output, the maximum numerical sample resistance and sample stiffness (initial slope of the load-displacement diagram) are almost aligned, so the numerical and experimental samples match relatively well, confirming that the numerical sample is validated against the experimental one.

3. Analysis of Findings

Due to the cost and limitations of structural experiments, the finite element method serves as an accurate and low-cost alternative for examining structural behavior. In this part of the study, micro-model analysis of the re-centering damper, including friction wedges and SMA rods is conducted to investigate the application of the re-centering damper in steel frames, the seismic performance of the re-centering damper, and the effects of the number and diameter of SMA rods, friction coefficient, and damper arrangement (series or parallel) on their seismic performance.

3.1. Application of the Re-centering Damper in Steel Frames

In this section, to apply the re-centering damper, including friction wedges and SMA rods in steel frames, necessary preparations were made to evaluate the actual performance of the damper at the frame scale. For this purpose, as per Figure 5, the holding chamber, steel connectors between the damper and connection plates, steel frame including beams, columns, and stiffeners, two diverging braces, and connection plates were designed and modeled, then transferred to ABAQUS for analysis. The steel frame with 2.34 m columns, 2.46 m beams, double IPE sections, and 120 mm channel sections for braces was assembled in ABAQUS's assembly module, then lateral loading coupling points and support conditions were defined to enable quasi-static analysis and cyclic loading.

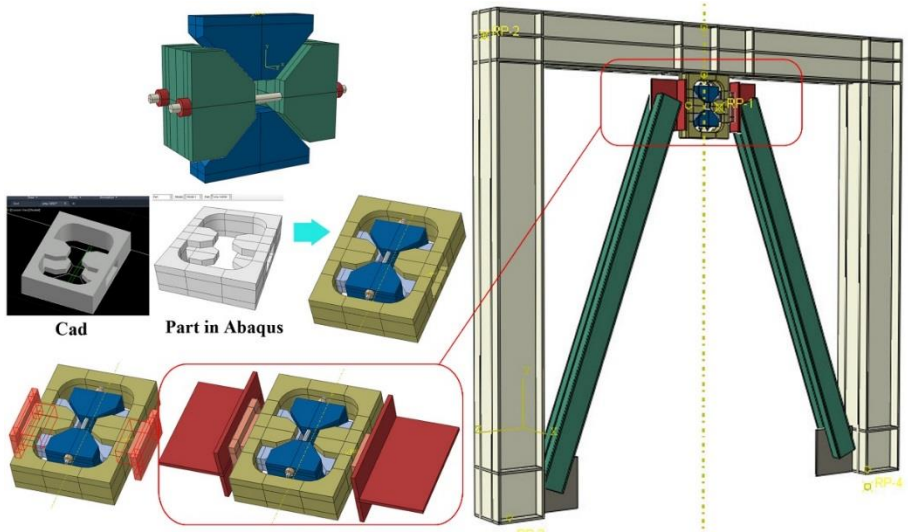

Figure 5- Design and modeling of steel frame components for applying the re-centering damper, including friction wedges and SMA rods.

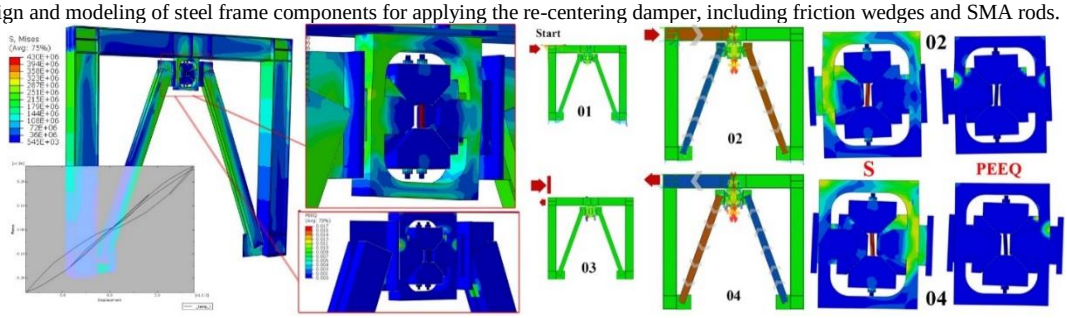

Figure 6- Stress and permanent deformations on the initial steel frame model with rigid connection to the re-centering damper assembly.

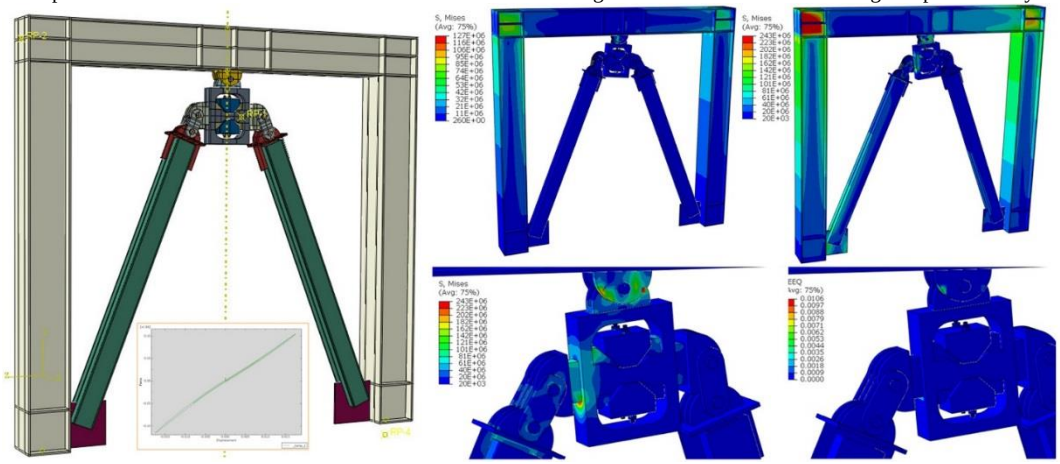

Figure 7- Stress on the secondary steel frame model with a hinged connection to the re-centering damper assembly

After modeling and assembly, in this stage, the re-centering damper with friction wedges and SMA rods is rigidly connected to the central beam in the steel frame, such that its proper performance is ensured when all deformations are concentrated in the SMA rods, absorbing and dissipating stresses while maintaining self-reversibility; otherwise, the placement and definition of the damper would be incorrect. Initial lateral loading results showed that although the load-displacement diagram, as per Figure 6, is flag-shaped and passes through the coordinate origin, some permanent deformation is observed at the brace ends and damper holding chamber due to rotation and additional moment. Stress vector analysis, as per Figure 6, also indicated that excessive rigidity of the chamber and connectors causes these permanent deformations.

To resolve this issue in the next stage, the connections of the damper holding chamber and steel connectors were designed as hinged as per Figure 7. The new analysis results indicate significant improvement in damper

performance, with no permanent deformation observed in frame members and the damper holding chamber, and the load-displacement diagram obtained is linear and fully reversible.

3.2. Seismic Performance of the Re-centering Damper

In this section, since reference samples are needed for comparison with other parametric samples, the seismic performance of the baseline re-centering damper in the study is first examined. This sample is based on the experimental model of Zhang et al. [2] but validated; the main difference from Zhang's model, as per Figure 8, is increasing the width of the upper and lower wedges from 4 to 12 cm and adding two extra SMA rods for effective performance in both compression and tension directions. Quasi-static analysis, as per Figure 8, showed that stresses on the rods are absorbed in both compressive and tensile states, and the damper acts as self-centering. The resulting load-displacement diagram shows flag-shaped and reversible behavior, indicating no permanent deformation. Then, by bilinearizing the load-displacement diagram using the equivalent energy method, seismic parameters including initial stiffness (slope of the line) (K), maximum resistance (P), and ductility (ratio of ultimate displacement to yield displacement) (μ) were extracted, as per Figure 8, serving as the basis for evaluating the seismic performance of the re-centering damper in this study. Note that the reference sample in this study is labeled "N2Q10F09*", where N2 means two rods connected to each wedge, Q10 means each damper rod diameter is 10 mm, and F09 means the initial friction coefficient between the two grooved wedge surfaces is 0.09. The asterisk denotes the reference sample.

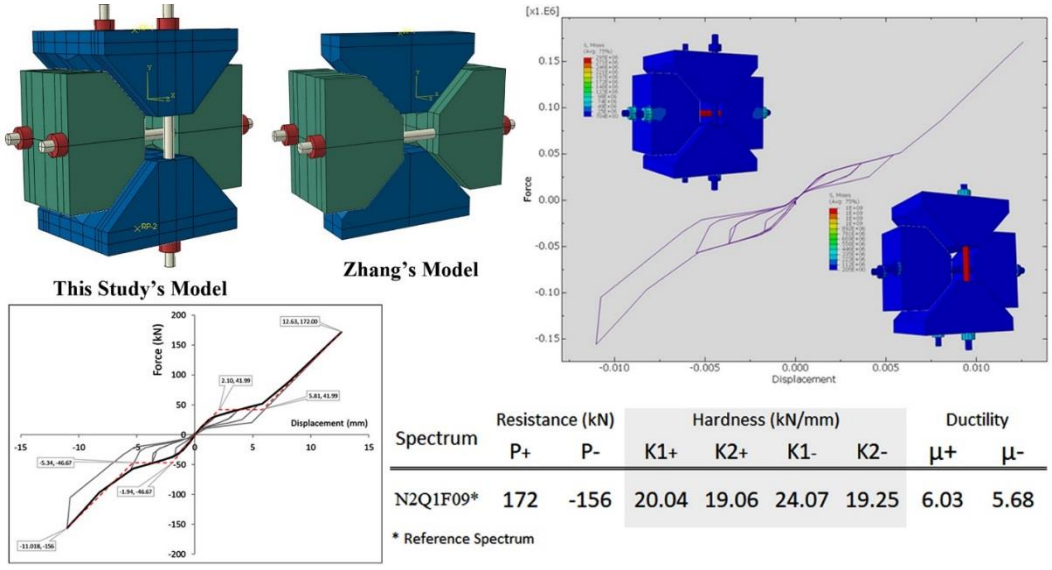

Spectrum	Resistance (kN)		Hardness (kN/mm)				Ductility	
	P+	P-	K1+	K2+	K1-	K2-	μ+	μ-
N2Q1F09*	172	-156	20.04	19.06	24.07	19.25	6.03	5.68

* Reference Spectrum

Figure 8- Results (stresses and performances) of hysteretic loading in both directions of the re-centering damper introduced in this study.

Table 1-
Results (stresses and performances) of hysteretic loading in both directions of the re-centering damper introduced in this study.

Spectrum	Number of SMA rods connected to each wedge	Diameter of each SMA rod (mm)	Coefficient of friction between two grooved wedge surfaces	Arrangement of two re-centering dampers relative to each other
N2Q10F09*	2	10	0.09	-
N3Q10F09	3	10	0.09	-
N4Q10F09	4	10	0.09	-
N2Q15F09	2	15	0.09	-
N2Q20F09	2	20	0.09	-
N2Q10F12	2	10	0.12	-
N2Q10F15	2	10	0.15	-
N2Q10F25	2	10	0.25	-
N2Q10F09-Se	2	10	0.09	Series
N2Q10F09-Pa	2	10	0.09	Parallel

* Reference Spectrum

3.3. Examination of Parametric Samples

In the continuation of the study, to examine parametric samples, the effects of the number and diameter of shape memory alloy rods, changes in friction coefficient between wedges, and the arrangement of two re-centering dampers relative to each other on the seismic performance of the re-centering damper, including friction wedges and SMA rods, are evaluated. Accordingly, Table 1 shows the naming of parametric samples with their specific features.

Table 1 displays variables regarding the number of shape memory alloy rods (2/3/4), diameter of each shape memory alloy rod (10/15/20 mm), friction coefficient between wedges (0.09/0.12/0.15/0.25), and arrangement of two re-centering dampers relative to each other (series/parallel), with modeling of these samples shown in Figure 9 and results of applied seismic hysteretic loading in Figure 10.

The results of back-and-forth hysteretic loading on parametric samples, as per Figure 10, show that increasing the number and diameter of SMA rods, as well as increasing the friction coefficient, increases the seismic resistance and stiffness of the re-centering damper but reduces its ductility. In a parallel configuration, resistance and stiffness are higher, but ductility is lower, whereas in a series configuration, all three parameters of resistance, stiffness, and ductility decrease. Consequently, increasing the resistance components improves load-bearing capacity but makes the damper behavior stiffer and less flexible. By

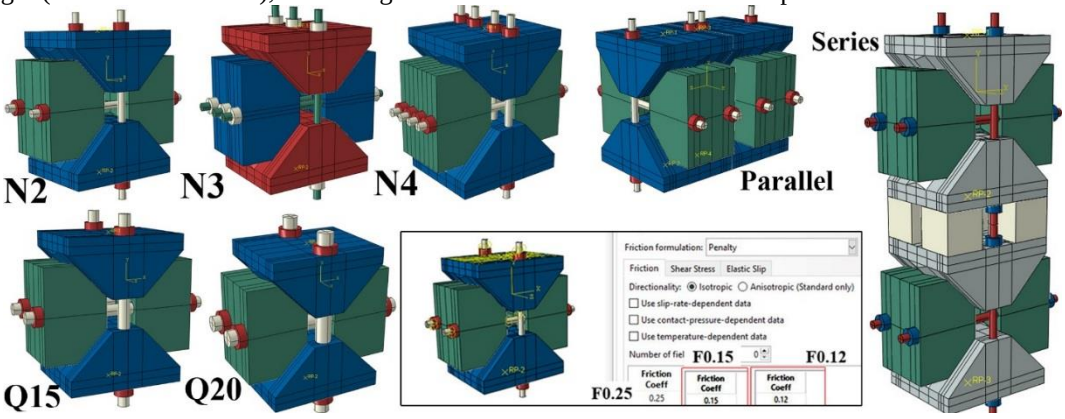

Figure 9- Display and introduction of parametric samples used in this study.

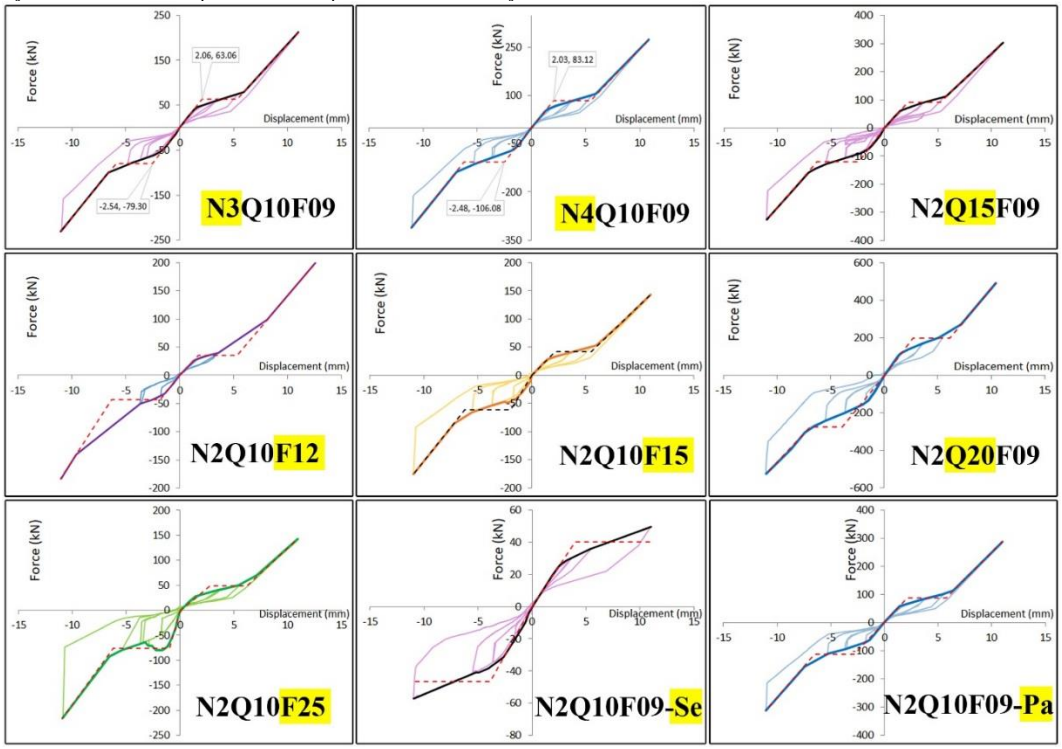

Figure 10- Results of applied seismic hysteretic loading on parametric samples.

Table 2
Details of seismic performance of parametric samples of the re-centering damper introduced in this study.

Spectrum	Resistance (kN)		Hardness (kN/mm)				Ductility	
	P+	P-	K1+	K2+	K1-	K2-	μ+	μ-
N2Q10F09*	172	-156	20.04	19.06	24.07	19.25	6.03	5.68
N3Q10F09	212	-230	30.59	26.00	31.18	29.43	5.35	4.34
N4Q10F09	275	-311	40.95	35.54	42.77	42.20	5.33	4.46
N2Q15F09	304	-326	42.10	36.14	49.57	43.85	5.06	4.53
N2Q20F09	491	-525	73.67	66.76	70.09	60.69	3.85	2.81
N2Q10F12	149	-183	22.85	22.54	25.44	29.64	7.21	5.98
N2Q10F15	143	-176	19.55	18.25	31.17	23.91	3.85	2.81
N2Q10F25	143	-216	17.54	19.73	77.54	29.56	3.90	11.21
N2Q10F09-Pa	287	-313	41.00	38.35	40.15	44.01	5.19	3.92
N2Q10F09-Se	49	-57	10.07	0	31.17	0	2.77	2.81

* Reference Spectrum

calculating the seismic performance of parametric samples, Table 2 details their performance.

Therefore, as per Table 2, the parametric examination results showed that increasing the number of SMA rods in the re-centering damper, including friction wedges and SMA rods, significantly improves seismic resistance and stiffness but reduces ductility. Specifically, increasing the number of rods from 2 to 3 and 4 increases seismic resistance in tension by 23% and 60%, and in compression by 4% and 100%, respectively. Initial seismic stiffness in tension increases by 52% and 100%, and in compression by 52% and 77%, while ductility in tension decreases by about 11% and in compression by 23% and 21%, respectively. As a result, increasing the number of rods leads to more resistant but brittle seismic performance in the re-centering damper, requiring a balance between resistance and ductility in design.

Additionally, the results of examining the effect of changing SMA rod diameter on the seismic performance of the re-centering damper showed that increasing rod diameter significantly increases damper seismic resistance and stiffness, such that increasing diameter from 1 cm to 1.5 and 2 cm increases seismic resistance in tension by 77% and 185%, and in compression by 109% and 237%, respectively. Initial seismic stiffness in tension increases by 110% and 268%, and in compression by 106% and 191%. However, seismic ductility decreases, in tension by 16% and 36%, and in compression by 20% and 51%. Therefore, increasing rod diameter improves damper resistance and stiffness but is accompanied by reduced ductility.

Furthermore, the results show that increasing the friction coefficient of friction wedges in the re-centering damper significantly increases seismic resistance and stiffness in the negative (compressive) section, while its effect on the positive (tensile) section is less noticeable, such that increasing the friction coefficient from 0.09 to 0.12, 0.15, and 0.25 increases seismic resistance in the positive section by 13%, 17%, and 17%, and in the negative section by 17%, 13%, and 39%, respectively. The initial seismic stiffness criterion in the positive section has minor changes, and in the negative section, especially at 0.25, increases up to 222%. Ductility in the positive section slightly increases or decreases with friction coefficient changes, and in the negative section shows more fluctuations (from 51% decrease to 97% increase). Overall, increasing the friction coefficient improves damper resistance and stiffness but reduces its ductility.

The examination of the effect of the placement status of two re-centering dampers, including friction wedges and SMA rods, showed that parallel placement leads to increased seismic resistance and stiffness and reduced ductility, while series placement causes a decrease in seismic resistance, stiffness, and ductility, and loss of secondary stiffness. Quantitatively, changing from series to parallel increases seismic resistance in the positive (tensile) section by up to 67% and in the negative (compressive) section by up to 101%, while ductility decreases in the positive section by up to 14% and in the negative by up to 31%. Therefore, according to the conclusion, parallel damper configuration is effective for enhancing structural resistance and stiffness, but at the cost of reduced ductility, and the series configuration for dampers is not recommended at all.

4. Overall Comparison of Results

In this section of the research, to comprehensively evaluate seismic performance, all samples of the re-centering damper, including friction wedges and SMA rods, were examined and compared. Accordingly, the seismic performance of the samples in terms of resistance, stiffness, and ductility in both positive (tensile) and negative (compressive) directions is analyzed, and by sorting data from highest to lowest values, bar charts related to resistance, stiffness in both positive and negative directions, and seismic ductility are shown in Figure 11.

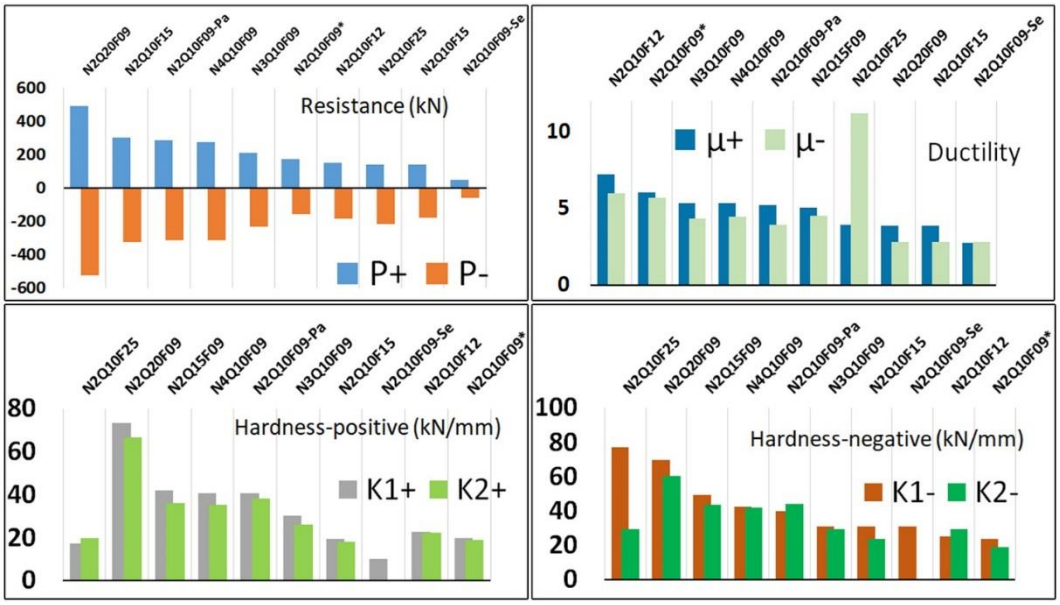

Figure 11- Bar chart results of comparative parametric samples in three criteria: resistance, stiffness, and seismic ductility.

The results of these charts provide a comprehensive view of the seismic behavior of different dampers and show that by simultaneously comparing the mentioned indices, the relative performance of each sample can be evaluated.

As per the bar chart results of comparative parametric samples in three criteria: resistance, stiffness, and seismic ductility in Figure 11, the following can be deduced:

- Based on the bar chart results, the highest seismic resistance was observed in samples N2Q20F09, N2Q15F09, and N2Q10F09-Pa, respectively, while the lowest resistance belonged to samples N2Q10F09-Se, N2Q10F15, and N2Q10F25, respectively.
- Also, in the tensile (positive) section of the bar chart, initial and secondary stiffness results (K1 and K2) showed that samples N2Q20F09, N2Q15F09, and N2Q10F09-Pa had the highest initial seismic stiffness, respectively, and samples N2Q10F09-Se, N2Q10F25, and N2Q10F15 had the lowest stiffness, respectively.
- In the compressive (negative) section of the bar chart, initial and secondary stiffness results (K1 and K2) showed that samples N2Q10F25, N2Q20F09, and N2Q15F09 had the highest stiffness, respectively, and samples N2Q10F09*, N2Q10F12, and N2Q10F09-Se had the lowest stiffness, respectively.
- In ductility evaluation, the highest performance belonged to samples N2Q10F12, N2Q10F09*, and N3Q10F09, and the lowest ductility was observed in samples N2Q10F09-Se, N2Q10F15, and N2Q20F09. Of course, the ductility criterion in the compressive (negative) section of the bar chart for sample N2Q10F25 differs greatly from other samples, and in this section, this sample has high ductility, which can be attributed to its feature, namely, a very high friction coefficient between the wedges.

5. Conclusion

In this research, aiming to improve the performance of re-centering dampers, the behavior of Zhang's damper was reviewed and numerically developed. By modifying the connection method and adding two SMA rods in the tension direction, full performance in compression and tension cycles was enabled. Then, the effects of parameters such as the number and diameter of SMA rods, wedge friction coefficient, and damper arrangement (series or parallel) on seismic resistance, stiffness, and ductility were examined, with the results of these analyses forming the basis for the final research conclusions as follows:

1. According to the examinations, it was determined that Zhang's re-centering damper assembly (designed only for the compressive section, stretching SMA rods with friction wedges) should not be rigidly connected to the lower part of the beam in chevron braces. For proper frame and damper performance, hinges must be provided between the damper chamber and brace, as well as at the lower part of the beam, to transfer lateral load without creating additional moment. Furthermore, in this study, by numerically developing Zhang's damper and adding two SMA rods directly in the tension direction through

increasing wedge width, the damper could create a full compression and tension cycle. The flag-shaped load-displacement diagram and its passage through the coordinate origin indicate the correct performance, reversibility, and re-centering of the new idea.

2. Parametric studies of the re-centering damper (in full compression and tension cycle) show that increasing the number and diameter of SMA rods increases seismic resistance and stiffness but decreases ductility. Also, increasing the friction coefficient of friction wedges, due to its direct effect on resistance and stiffness in the compressive section, increases seismic resistance and stiffness in the compressive section, while no noticeable change is seen in the tensile section, but overall, damper ductility decreases.
3. Parametric study results of the re-centering damper (in full compression and tension cycle) show that in parallel configuration, seismic resistance and stiffness increase, but ductility decreases. It was also observed that parallel configuration results are almost equal to the case with 4 rods, concluding no difference between parallel dampers and using four rods. In contrast, in a series configuration, resistance, stiffness, and ductility significantly decrease; therefore, using a series configuration for the re-centering damper is not recommended at all.
4. Post-analysis phase results of this research show that the effect of increasing damper diameter on seismic performance (resistance and stiffness) is much greater than increasing the number and friction coefficient, and excessive increase in friction between wedges only increases initial seismic stiffness in the compression section but simultaneously reduces seismic resistance.
5. Additionally, post-analysis phase results of this research show that if the friction coefficient approaches 0.12, it has higher seismic ductility than the baseline sample with a 0.09 friction coefficient, and overall, all reinforced samples have lower ductility compared to the baseline sample

References

[1] Almajhali, K. Y. M. "Review of passive energy dissipation devices and techniques of installation for high-rise building structures." Structures 51 (2023): 1019-1029. https://doi.org/10.1016/j.istruc.2023.03.025

[2] Zhang, H., A. Li, Y. Su, G. Xu, and B. Sha. "Viscoelastic dampers for civil engineering structures: A systematic review of constructions, materials, and applications." Journal of Building Engineering 96 (2024): 110597. https://doi.org/10.1016/j.jobe.2024.110597

[3] Avşar, Ö., S. Cao, and O. E. Ozbulut. "Development and characterization of self-centering friction dampers with confined shape memory alloy bars." Journal of Building Engineering 90 (2024): 109504. https://doi.org/10.1016/j.jobe.2024.109504

[4] Riaz, R. D., U. J. Malik, M. U. Shah, M. Usman, and F. A. Najam. "Enhancing Seismic Resilience of Existing Reinforced Concrete Building Using Non-Linear Viscous Dampers: A Comparative Study." Actuators 12.4 (2023): 175. https://doi.org/10.3390/act12040175

[5] Jiang, H., Z. Huang, and H. N. Li. "Deformation-amplified self-centering energy-dissipation device for seismic control: Design, testing and simulation." Engineering Structures 280 (2023): 115671. https://doi.org/10.1016/j.engstruct.2023.115671

[6] Mohammadgholipour, A., and A. H. M. M. Billah. "Mechanical properties and constitutive models of shape memory alloy for structural engineering: A review." Journal of Intelligent Material Systems and Structures 34.20 (2023): 2335-2359. https://doi.org/10.1177/1045389X231185458

[7] Fang, C., C. Qiu, and Y. Zheng. "Shape memory alloys for civil engineering." Materials 16.2 (2023): 787. https://doi.org/10.3390/ma16020787

[8] Zhang, S., H. Hou, B. Qu, Y. Zhu, K. Li, and X. Fu. "Tests of a novel re-centering damper with SMA rods and friction wedges." Engineering Structures 245 (2021): 112125. https://doi.org/10.1016/j.engstruct.2021.112125

[9] Asfaw, A. M., L. Cao, O. E. Ozbulut, and J. Ricles. "Development of a shape memory alloy-based friction damper and its experimental characterization considering rate and temperature effects." Engineering Structures 270 (2022): 115101. https://doi.org/10.1016/j.engstruct.2022.115101

[10] Mohammadi Nia, M., S. Moradi, and T. Yang. "Performance-based seismic design of self-centering steel moment frames with SMA-bolted connections." Journal of Constructional Steel Research 208 (2023): 107990. https://doi.org/10.1016/j.jcsr.2023.107990

[11] Wang, B., and S. Zhu. "Superelastic SMA U-shaped dampers with self-centering functions." Smart Materials and Structures 27.5 (2018): 055003. https://doi.org/10.1088/1361-665X/aab52d

[12] ABAQUS-V6.19-1. "Finite Element Analysis Software." Johnston, RI, USA. ABAQUS/Standard theory. Manual, Dassault Systèmes Simulia Corp., 2019.